Article

Aminoglycoside Complexation with a DNA·RNA Hybrid Duplex: The Thermodynamics of Recognition and Inhibition of RNA Processing Enzymes

Christopher M. Barbieri, Tsai-Kun Li, Susan Guo, Gang Wang, Anthony J. Shallop, Weidong Pan, Gengcheng Yang, Barbara L. Gaffney, Roger A. Jones, and Daniel S. Pilch

J. Am. Chem. Soc., **2003**, 125 (21), 6469-6477• DOI: 10.1021/ja021371d • Publication Date (Web): 02 May 2003

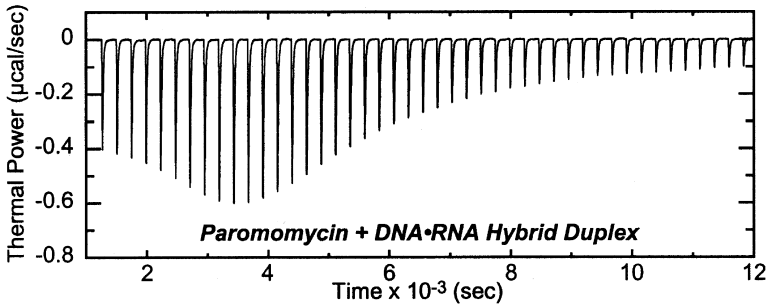

More About This Article

Additional resources and features associated with this article are available within the HTML version:

- Supporting Information
- Links to the 1 articles that cite this article, as of the time of this article download
- Access to high resolution figures
- Links to articles and content related to this article
- Copyright permission to reproduce figures and/or text from this article

View the Full Text HTML

J|A|C|S
ARTICLES
Published on Web 05/02/2003

Aminoglycoside Complexation with a DNA·RNA Hybrid Duplex: The Thermodynamics of Recognition and Inhibition of RNA Processing Enzymes

Christopher M. Barbieri,[†] Tsai-Kun Li,[†] Susan Guo,[†] Gang Wang,[‡] Anthony J. Shallop,[‡] Weidong Pan,[‡] Gengcheng Yang,[‡] Barbara L. Gaffney,[‡] Roger A. Jones,[‡] and Daniel S. Pilch*[,†,§]

Contribution from the Department of Pharmacology, University of Medicine and Dentistry of New Jersey-Robert Wood Johnson Medical School, 675 Hoes Lane, Piscataway, New Jersey 08854-5635; the Department of Chemistry and Chemical Biology, Rutgers-The State University of New Jersey, 610 Taylor Road, Piscataway, New Jersey 08854-8087; and The Cancer Institute of New Jersey, New Brunswick, New Jersey 08901

Received November 22, 2002; E-mail: pilchds@umdnj.edu

Abstract: Spectroscopic and calorimetric techniques were employed to characterize and contrast the binding of the aminoglycoside paromomycin to three octamer nucleic acid duplexes of identical sequence but different strand composition (a DNA·RNA hybrid duplex and the corresponding DNA·DNA and RNA·RNA duplexes). In addition, the impact of paromomycin binding on both RNase H- and RNase A-mediated cleavage of the RNA strand in the DNA·RNA duplex was also determined. Our results reveal the following significant features: (i) Paromomycin binding enhances the thermal stabilities of the RNA·RNA and DNA·RNA duplexes to similar extents, with this thermal enhancement being substantially greater in magnitude than that of the DNA·DNA duplex. (ii) Paromomycin binding to the DNA·RNA hybrid duplex induces CD changes consistent with a shift from an A-like to a more canonical A-conformation. (iii) Paromomycin binding to all three octamer duplexes is linked to the uptake of a similar number of protons, with the magnitude of this number being dependent on pH. (iv) The affinity of paromomycin for the three host duplexes follows the hierarchy, RNA·RNA > DNA·RNA ≫ DNA·DNA. (v) The observed affinity of paromomycin for the RNA·RNA and DNA·RNA duplexes decreases with increasing pH. (vi) The binding of paromomycin to the DNA·RNA hybrid duplex inhibits both RNase H- and RNase A-mediated cleavage of the RNA strand. We discuss the implications of our combined results with regard to the specific targeting of DNA·RNA hybrid duplex domains and potential antiretroviral applications.

Introduction

The aminoglycosides are a family of antibiotics whose bactericidal activities are derived from their abilities to form a complex with the small ribosomal subunit, thereby interfering with protein synthesis.[1,2] The majority of aminoglycosides contain the aminocyclitol moiety, 2-deoxystreptamine (2-DOS). Aminoglycosides of the 2-DOS family specifically target conserved sequences in the A site of the 16 S ribosomal RNA (rRNA) subunit.[3−5] In recent years, the array of RNA structures that can be targeted by the aminoglycosides has increased considerably. These RNA structures include ribozymes, protein binding elements, aptamers, and polymeric duplexes.[6−9] NMR and crystallographic studies on several aminoglycoside-RNA complexes have provided some key insights into the structural nature of the drug binding sites.[10−15] One of the common features to emerge from the structural studies of aminoglycoside-RNA interactions is the major groove-directed mode of complexation. In many cases, the sequence of the host RNA dictates a specific structural motif or conformation that, in turn, serves as a specific recognition element for the aminoglycoside. Formation of the specific aminoglycoside binding site can be

[†] UMDNJ-Robert Wood Johnson Medical School.
[‡] Rutgers University.
[§] The Cancer Institute of New Jersey.

(1) Carter, A. P.; Clemons, W. M.; Brodersen, D. E.; Morgan-Warren, R. J.; Wimberly, B. T.; Ramakrishnan, V. *Nature* **2000**, *407*, 340−348.
(2) Puglisi, J. D.; Blanchard, S. C.; Dahlquist, K. D.; Eason, R. G.; Fourmy, D.; Lynch, S. R.; Recht, M. I.; Yoshizawa, S. In *The Ribosome: Structure, Function, Antibiotics, and Cellular Interactions*; Garrett, R. A., Douthwaite, S. R., Liljas, A., Metheson, A. T., Moore, P. B., Noller, H. F., Eds.; ASM Press: Washington, DC, 2000; pp 419−429.
(3) Moazed, D.; Noller, H. F. *Nature* **1987**, *327*, 389−394.
(4) Woodcock, J.; Moazed, D.; Cannon, M.; Davies, J.; Noller, H. F. *EMBO J.* **1991**, *10*, 3099−3103.
(5) Gutell, R. R. *Nucleic Acids Res.* **1994**, *22*, 3502−3507.
(6) Wallis, M. G.; Schroeder, R. *Prog. Biophys. Mol. Biol.* **1997**, *67*, 141−154.
(7) Michael, K.; Tor, Y. *Chem. Eur. J.* **1998**, *4*, 2091−2098.
(8) Tor, Y. *Angew. Chem., Int. Ed. Engl.* **1999**, *38*, 1579−1582.
(9) Schroeder, R.; Waldsich, C.; Wank, H. *EMBO J.* **2000**, *19*, 1−9.
(10) Fourmy, D.; Recht, M. I.; Blanchard, S. C.; Puglisi, J. D. *Science* **1996**, *274*, 1367−1371.
(11) Jiang, L.; Suri, A. K.; Fiala, R.; Patel, D. J. *Chem. Biol.* **1997**, *4*, 35−50.
(12) Jiang, L.; Patel, D. J. *Nature Struct. Biol.* **1998**, *5*, 769−774.
(13) Yoshizawa, S.; Fourmy, D.; Puglisi, J. D. *EMBO J.* **1998**, *17*, 6437−6448.
(14) Vicens, Q.; Westhof, E. *Structure* **2001**, *9*, 647−658.
(15) Vicens, Q.; Westhof, E. *Chem. Biol.* **2002**, *9*, 747−755.

dependent on a drug-induced conformational change in the host RNA, as has been demonstrated for aminoglycoside complexation with the A site of 16 S rRNA.[10,13−16]

Recent studies by the Shafer group have shown that the aminoglycosides lividomycin A, neomycin B, and kanamycin B enhance the thermal stabilities of polymeric RNA duplexes to a significantly greater extent than the corresponding polymeric DNA duplexes,[17] an observation that was later recapitulated by Arya and co-workers.[18] On the basis of these results, as well as those described above, it is tempting to classify the aminoglycosides as RNA-specific nucleic acid binding ligands. However, several recent studies have indicated that the nucleic acid binding specificity of the aminoglycosides is not for RNA, but rather for the A-conformation. First, NMR studies by the Wang group have demonstrated that neomycin B can induce the B-to-A transition in G·C-rich oligomeric DNA duplexes,[19] a behavior that is also exhibited by the cationic ligands, $Co(NH_3)_6^{3+}$ and spermine.[19,20] Significantly, these studies also revealed that the three ligands share a common structural basis for their induction of the B-to-A transition, which involves discrete interactions between the ligand and the major groove of the host DNA. Second, CD and NMR studies by the Shafer group have shown that lividomycin A facilitates the ethanol-induced B-to-A transition in calf thymus DNA through its interactions with the major groove of the host duplex.[17] Third, neomycin significantly enhances the thermal stability of the poly(dA)·2poly(dT) triplex, which is known to adopt an A-like conformation,[21,22] while having little or no effect on the thermal stability of the corresponding poly(dA)·poly(dT) duplex.[18]

The specificity exhibited by aminoglycosides for the A-conformation raises the possibility that these drugs may be able to target RNA·DNA hybrid duplexes, which adopt A-like structures.[23] The potential of RNA·DNA hybrids to serve as aminoglycoside targets has been highlighted by the recent observation that a number of different 2-DOS aminoglycosides (including neomycin, paromomycin, and tobramycin) enhance the thermal stability of the poly(rA)·poly(dT) duplex.[24] The targeting of RNA·DNA hybrid structures with small molecules offers the potential for modulating specific biochemical processes.[24,25] One such process is RNase H-mediated RNA cleavage, an activity exhibited by retroviral reverse transcriptases that is essential for viral replication.[26]

Here, we use a combination of spectroscopic and calorimetric techniques to characterize and contrast the binding of the aminoglycoside paromomycin I (hereafter denoted as paromomycin) to an octameric RNA·DNA hybrid duplex versus the corresponding DNA·DNA and RNA·RNA duplexes of the same sequence (see Figure 1 for the sequences of the RNA and DNA octamers used in this study, as well as for the structure of paromomycin). The sequence of the RNA strand in the RNA·DNA hybrid duplex studied here is derived from the HIV-1 genome and consists of the four bases at the 3′-end of the U5 region and the four bases at the 5′-end of the primer binding site (PBS).[27] This sequence was selected because it includes a specific RNase H cleavage site for the reverse transcriptase enzyme of HIV-1.[28] Our results demonstrate that the affinity of paromomycin for the RNA·DNA and RNA·RNA duplexes is substantially greater (≥187-fold) than that for the DNA·DNA duplex. Furthermore, the binding of paromomycin to the RNA·DNA hybrid duplex induces a conformational transition from an A-like to a more canonical A-conformation, consistent with an A-form binding specificity. Our results also reveal that the binding of paromomycin to the RNA·DNA hybrid duplex antagonizes both RNase H- and RNase A-mediated cleavage of the RNA strand. We discuss the implications of our results with regard to the specific targeting of RNA·DNA hybrid duplex domains and potential antiretroviral applications.

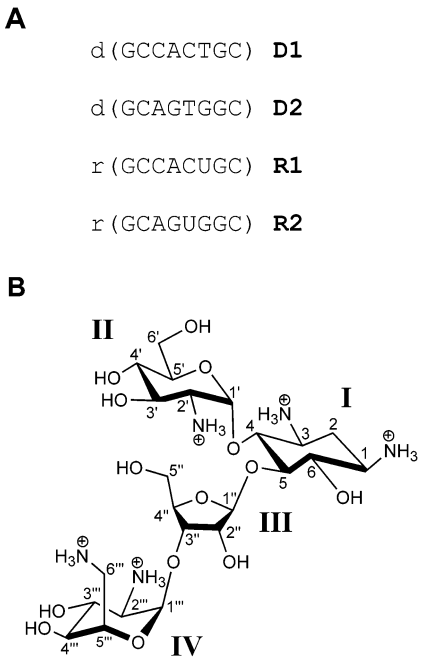

Figure 1. (A) Base sequences of the two DNA (lower case "d") and two RNA (lower case "r") octamers used in this study. (B) The chemical structure of paromomycin I, with the ring numbering indicated in Roman numerals and the atomic numbering indicated in Arabic numerals.

Materials and Methods

Enzyme, Nucleic Acid, and Drug Molecules. The D1 and D2 DNA oligonucleotides were synthesized using standard phosphoramidite procedures. The R1 and R2 RNA oligonucleotides were synthesized using phosphoramidites protected as previously described.[29] The final deprotection and purification strategy used for these RNA oligonucleotides was described earlier.[30] Paromomycin sulfate was obtained from

(16) Fourmy, D.; Yoshizawa, S.; Puglisi, J. D. *J. Mol. Biol.* **1998**, *277*, 333−345.
(17) Chen, Q.; Shafer, R. H.; Kuntz, I. D. *Biochemistry* **1997**, *36*, 11 402−11 407.
(18) Arya, D. P.; Coffee, R. L., Jr.; Willis, B.; Abramovitch, A. I. *J. Am. Chem. Soc.* **2001**, *123*, 5385−5395.
(19) Robinson, H.; Wang, A. H.-J. *Nucleic Acids Res.* **1996**, *24*, 676−682.
(20) Xu, Q.; Shoemaker, R. K.; Braunlin, W. H. *Biophys. J.* **1993**, *65*, 1039−1049.
(21) Arnott, S.; Selsing, E. *J. Mol. Biol.* **1974**, *88*, 509−521.
(22) Arnott, S.; Bond, P. J.; Selsing, E.; Smith, P. J. C. *Nucleic Acids Res.* **1976**, *3*, 2459−2470.
(23) Saenger, W. *Principles of Nucleic Acid Structure*; Springer-Verlag: New York, 1983.
(24) Arya, D. P.; Coffee, R. L., Jr.; Charles, I. *J. Am. Chem. Soc.* **2001**, *123*, 11 093−11 094.
(25) Ren, J.; Qu, X.; Dattagupta, N.; Chaires, J. B. *J. Am. Chem. Soc.* **2001**, *123*, 6742−6743.
(26) Larder, B. A. In *Reverse Transcriptase*; Goff, S. P., Ed.; Cold Spring Harbor Laboratory Press: New York, 1993; pp 205−222.
(27) Mueller, U.; Maier, G.; Onori, A. M.; Cellai, L.; Heumann, H.; Heinemann, U. *Biochemistry* **1998**, *37*, 12 005−12 011.
(28) Götte, M.; Fackler, S.; Hermann, T.; Perola, E.; Cellai, L.; Gross, H. J.; Le Grice, S. F. J.; Heumann, H. *EMBO Journal* **1995**, *14*, 833−841.
(29) Song, Q.; Wang, W.; Fischer, A.; Zhang, X.; Gaffney, B. L.; Jones, R. A. *Tetrahedron Lett.* **1999**, *40*, 4153−4156.

Fluka and used without further purification. Recombinant *E. coli* RNase H was obtained from USB, while bovine pancreas RNase A was obtained from Sigma.

UV Absorption Spectrophotometry. All UV absorbance experiments were conducted on an AVIV Model 14DS Spectrophotometer (Aviv Associates; Lakewood, NJ) equipped with a thermoelectrically controlled cell holder. A quartz cell with a 1 cm path length was used for all the absorbance studies. Absorbance versus temperature profiles were measured at 274 nm with a 6 s averaging time. The temperature was raised in 0.5 °C increments, and the samples were allowed to equilibrate for 1 min at each temperature setting. In these thermal denaturation studies, nucleic acid solutions were 10 μM in duplex and contained paromomycin at concentrations ranging from 0 to 30 μM. The buffer solutions for the UV melting experiments contained 10 mM sodium cacodylate (pH 6.0), 0.1 mM Na_2EDTA, and sufficient NaCl to bring the total Na^+ concentration to 60 mM. For each optically detected thermal transition, the melting temperature (T_m) was determined as previously described.[31]

Circular Dichroism (CD) Spectropolarimetry. CD experiments were conducted at 15 °C on an AVIV Model 60DS spectropolarimeter (Aviv Associates; Lakewood, NJ) equipped with a thermoelectrically controlled cell holder. A quartz cell with a 1 cm path length was used for all the CD studies. CD spectra were recorded from 230 to 320 nm in 1 nm increments with an averaging time of 2 s. The titrations were performed by incrementally adding 11 μL aliquots of 1 mM paromomycin into a nucleic acid solution (2.2 mL) that was 10 μM in duplex. Following each drug addition, the sample was allowed to equilibrate for 3 min prior to acquisition of the CD spectrum. The buffer conditions for the CD titrations were identical to those described above for the UV melting experiments. The final CD spectra for the titration were normalized to reflect equimolar duplex concentrations.

Isothermal Titration Calorimetry (ITC). Isothermal calorimetric measurements were performed at 15 °C on a MicroCal VP−ITC (MicroCal, Inc., Northampton, MA). In a typical experiment, 5 μL aliquots of 500 μM paromomycin were injected from a 250 μL rotating (300 rpm) syringe into an isothermal sample chamber containing 1.42 mL of a solution containing either D1·D2, R1·R2, or D1·R2 that was 20 μM in duplex. Each experiment of this type was accompanied by the corresponding control experiment in which the drug was injected into a solution of buffer alone. The duration of each injection was 5 s and the delay between injections was 240 s. The initial delay prior to the first injection was 60 s. Each injection generated a heat burst curve (μcal/sec vs sec). The area under each heat burst curve was determined by integration [using the Origin version 5.0 software (MicroCal, Inc., Northampton, MA)] to obtain a measure of the heat associated with that injection. The heat associated with each drug-buffer injection was subtracted from the corresponding heat associated with each drug-duplex injection to yield the heat of drug binding for that injection. The resulting corrected injection heats were plotted as a function of the [drug]/[duplex] ratio and fit with a model for either one set or two sets of binding sites using the MicroCal Origin version 5.0 software. The calorimeter was calibrated both electronically and chemically as described previously.[32] The buffer solutions for the ITC experiments contained either 10 mM sodium cacodylate, 10 mM MES, or 10 mM PIPES, as well as 0.1 mM Na_2EDTA. In addition, each solution contained sufficient NaCl to bring the total Na^+ concentration to 60 mM. The pH values of the ITC experimental solutions were either 6.0 or 7.0.

RNase A Cleavage Assay. The RNase A activity of bovine pancreas RNase A was assayed in a 10 μL reaction mixture containing 10 mM PIPES (pH 6.0) and 5 mM $MgCl_2$. 10 pmol of R2 were ^{32}P-labeled at the 5′-end using T4 polynucleotide kinase. Different concentrations of paromomycin, ranging from 0.0625 to 1.0 mM, were mixed with 0.5 μM of D1·R2. 10 pg of enzyme then were added to initiate the cleavage reaction. After incubation at 37 °C for 30 min, the reaction was stopped by addition of 3 M urea containing a mixture of bromophenol blue and xylene cyanol. The cleavage products were resolved in a 15% polyacrylamide gel containing 8 M urea. The gels were subsequently analyzed using a phosphoimager (Molecular Dynamics, Inc.).

RNase H Cleavage Assay. The RNase H activity of recombinant *E. coli* RNase H was assayed in a 10 μL reaction mixture containing the same buffer described above for the RNase A experiments. R2 was ^{32}P-labeled as described above. Different concentrations of paromomycin, ranging from 0.05 to 0.4 mM, were mixed with 0.5 μM of D1·R2. Two units of enzyme then were added to initiate the cleavage reaction. After incubation at room temperature for 1 h, the reaction was stopped as described above. The cleavage products were subsequently resolved and analyzed as described above.

Results and Discussion

Paromomycin Binding Enhances the Thermal Stabilities of the R1·R2 and D1·R2 Duplexes to a Similar Extent, with this Thermal Enhancement being Substantially Greater in Magnitude than that of the D1·D2 Duplex. UV melting experiments were conducted in the absence and presence of paromomycin to assess the impact, if any, of the drug on the thermal stabilities of the D1·D2, R1·R2, and D1·R2 duplexes. The resulting melting profiles are shown in Figure 2. Inspection of this figure reveals several features worthy of note. (i) The thermal stabilities (T_m) of the three drug-free duplexes follow the hierarchy, R1·R2 (T_m = 55.8 °C) > D1·R2 (T_m = 43.9 °C) > D1·D2 (T_m = 41.6 °C). Thus, duplex thermal stability depends on strand composition (RNA versus DNA). Note that our observed hierarchy of duplex thermal stability is consistent with that previously observed by Gyi et al.[33] in studies on a series of decamer duplexes containing both purine-rich and pyrimidine-rich DNA and RNA strands. (ii) The presence of paromomycin enhances the thermal stability of each duplex, an observation consistent with paromomycin binding to each of the target duplexes with a preference for the double- versus single-stranded state.[34] (iii) The extent to which paromomycin binding enhances duplex thermal stability (ΔT_m) follows the hierarchy, R1·R2 ≈ D1·R2 ≫ D1·D2. Specifically, paromomycin binding enhances the thermal stability of the all-RNA duplex and corresponding RNA·DNA hybrid duplex to a similar extent (ΔT_m = 6.3 and 6.2 °C, respectively), with this extent being substantially greater than that of the corresponding all-DNA duplex (ΔT_m = 0.8 °C). Thus, as measured by differences in ΔT_m, paromomycin preferentially targets the RNA·RNA and RNA·DNA hybrid duplexes relative to the DNA·DNA duplex, an observation confirmed by our ITC-derived binding affinities discussed in a later section.

Paromomycin Binding to the D1·R2 Hybrid Duplex Induces CD Changes Consistent with a Shift to a More Canonical A-Conformation. Figure 3A shows the CD spectra from 230 to 320 nm of the R1·R2, D1·R2, and D1·D2 duplexes in the absence of paromomycin. The CD spectrum of the D1·D2 duplex exhibits a negative band at 254 nm and a positive band at 285 nm, with these two bands being similar in

(30) Song, Q.; Jones, R. A. *Tetrahedron Lett.* **1999**, *40*, 4653−4654.
(31) Marky, L. A.; Breslauer, K. J. *Biopolymers* **1987**, *26*, 1601−1620.
(32) Pilch, D. S.; Kirolos, M. A.; Liu, X.; Plum, G. E.; Breslauer, K. J. *Biochemistry* **1995**, *34*, 9962−9976.
(33) Gyi, J. I.; Conn, G. L.; Lane, A. N.; Brown, T. *Biochemistry* **1996**, *35*, 12 538−12 548.
(34) McGhee, J. D. *Biopolymers* **1976**, *15*, 1345−1375.

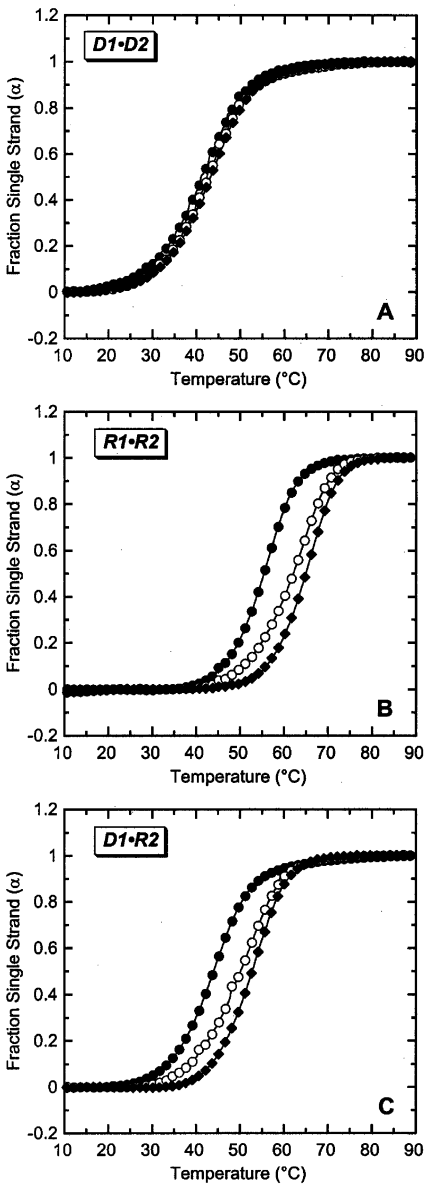

Figure 2. UV melting profiles for the D1·D2 (A), R1·R2 (B), and D1·R2 (C) duplexes in the presence and absence of paromomycin, with the [drug]/[duplex] ratios (r_{dup}) being 0 (filled circles), 1.0 (open circles), and 2.0 (filled diamonds). For clarity of presentation, the melting curves were normalized by subtraction of the upper and lower baselines to yield plots of fraction single strand (α) versus temperature.[31] All the UV melting profiles were acquired at 274 nm.

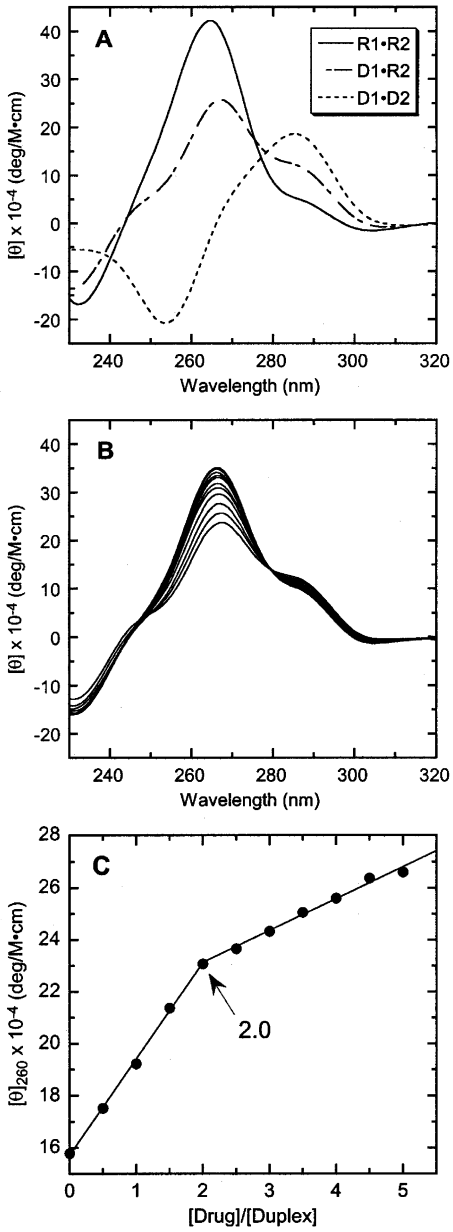

Figure 3. (A) CD spectra (at 15 °C) of the R1·R2, D1·R2, and D1·D2 duplexes (10 μM) in the absence of paromomycin. (B) CD titration of D1·R2 (10 μM) with paromomycin at 15 °C. From bottom to top at 265 nm, the CD spectra correspond to [drug]/[duplex] ratios (r_{dup}) ranging from 0 to 5.0 in increments of 0.5. (C) Molar ellipticity at 260 nm ($[\theta]_{260}$) as a function of the [drug]/[duplex] ratio for the titration of D1·R2 with paromomycin. The solid lines reflect the linear least-squares fits of each apparent linear domain of the experimental data (filled circles) before and after the apparent inflection point. The [drug]/[duplex] ratio (2.0) corresponding to the apparent inflection point is indicated. Molar ellipticity is expressed in units of deg/M·cm, where M refers to moles of nucleic acid duplex per liter.

magnitude. This semiconservative CD spectrum is typical of a canonical B-conformation.[35−37] The CD spectrum of the R1·R2 duplex exhibits a large positive band at 265 nm and a comparatively small negative band at 304 nm. These CD spectral properties are characteristic of a canonical A-conformation.[35−37] The CD spectrum of the D1·R2 hybrid duplex exhibits a large positive band at 266 nm, a smaller positive band at 288 nm, and a small negative band at 304 nm. This CD spectrum is not typical of a canonical A-conformation nor is it typical of a canonical B-conformation.[35−37] Instead, it is characteristic of a conformation that is intermediate between the B- and A-forms, but closer to the A-conformation.[33,35−37]

Figure 3B shows the CD spectra obtained by incremental titration of paromomycin into a solution of D1·R2. Note that addition of the drug alters the CD spectrum of the host duplex. These changes in duplex CD properties are indicative of interactions between paromomycin and the host duplex, and can be used to detect and monitor paromomycin binding. The paromomycin-induced changes in the CD spectrum of the

(35) Ivanov, V. I.; Minchenkova, L. E.; Schyolkina, A. K.; Poletayev, A. I. *Biopolymers* **1973**, *12*, 89−110.
(36) Gray, D. M.; Ratliff, R. L. *Biopolymers* **1975**, *14*, 487−498.
(37) Gray, D. M.; Ratliff, R. L.; Vaughan, M. R. *Methods Enzymol.* **1992**, *211*, 389−406.

D1·R2 duplex include increases in the intensities of both the positive band at 266 nm and the negative band at 304 nm, as well as a decrease in the intensity of the positive band at 288 nm. These CD spectral changes are consistent with a paromomycin-induced shift from an A-like to a more canonical A-conformation.[35−37] In other words, our CD data are consistent with the preferential binding of paromomycin to A-form versus B-form nucleic acid duplexes. Further inspection of the CD spectra in Figure 3B reveals the presence of an isoelliptic point at 279 nm. The presence of a single isoelliptic point is consistent with a single CD-detectable mode of paromomycin binding when D1·R2 serves as the host duplex.

Figure 3C shows a titration curve at 260 nm extracted from the family of CD spectra shown in Figure 3B. In this curve, the data points represent the experimental molar ellipticities of the host duplex, whereas the solid lines reflect linear least-squares fits of each apparent linear domain of the experimental data. Note the presence of a single inflection point in the titration curve, with this inflection point corresponding to a [drug]/[duplex] ratio of 2.0. This observation is consistent with an overall binding stoichiometry of two paromomycin molecules per D1·R2 duplex, a stoichiometry confirmed by ITC studies described in a later section.

At pH 6.0, Paromomycin Binds to the D1·R2 Hybrid Duplex with a 3.7-Fold Lower Affinity than the Corresponding R1·R2 RNA Duplex and a 187-Fold Higher Affinity than the Corresponding D1·D2 DNA Duplex. We used ITC to further characterize the binding of paromomycin to the three target duplexes studied here. The resulting ITC profiles derived from experiments conducted in cacodylate buffer at pH 6.0 and 15 °C are shown in Figure 4. Each of the heat burst curves in Figure 4 corresponds to a single paromomycin injection. The areas under these heat burst curves were determined by integration to yield the associated injection heats. These injection heats were corrected by subtraction of the corresponding dilution heats derived from the injection of identical amounts of paromomycin into buffer alone and then plotted as a function of r_{dup}. The resulting plots are shown in Figure 5. Note that the plot resulting from the complexation of paromomycin with the D1·D2 duplex (Figure 5A) is monophasic. By contrast, the corresponding plots resulting from the interaction of paromomycin with the R1·R2 (Figure 5B) and D1·R2 (Figure 5C) duplexes are biphasic. These observations indicate that the complexation of paromomycin with the D1·D2 duplex can be described by a single binding equilibrium, while the complexation of paromomycin with the R1·R2 and D1·R2 duplexes can be described by two distinct binding equilibria. In this connection, the injection heat data in Figure 5A were fit with a model for one set of binding sites, while the corresponding data in Figure 5B and C were fit with a model for two independent sets of binding sites. The resulting fits, which were calculated using the MicroCal Origin 5.0 software suite, are depicted as solid lines in Figure 5. For the acquisition of these fits, the paromomycin-duplex association constant (K_a) and the observed binding enthalpy (ΔH_{obs}) were used as free-floating parameters, while the drug-duplex binding stoichiometry (N) was fixed during the fitting routine and manually varied to yield the best fit. Table 1 summarizes the values of K_a, ΔH_{obs}, and N derived from the fits of the data shown in Figure 5. Note that the overall binding stoichiometry (N) for paromomycin complexation with

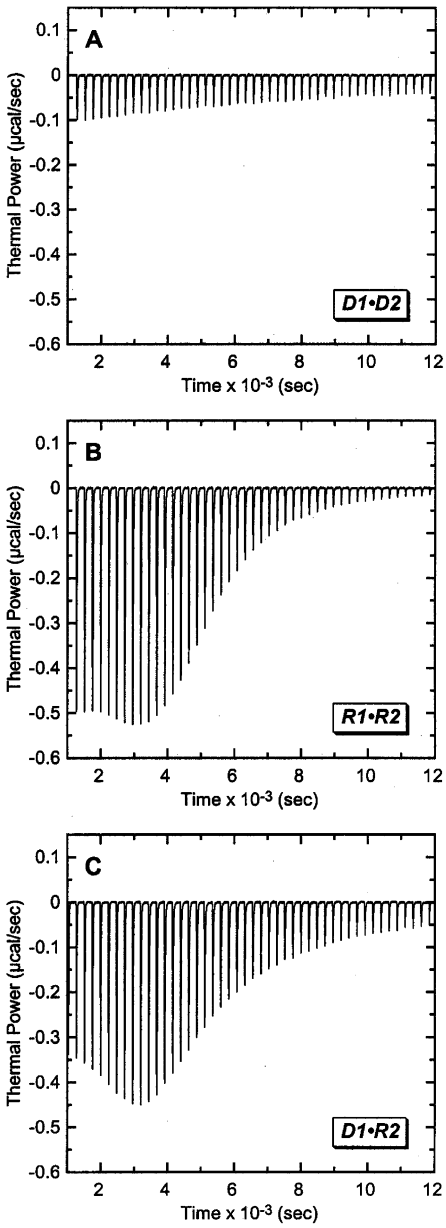

Figure 4. ITC profiles at 15 °C and pH 6.0 for the titration of paromomycin into a solution containing the D1·D2 (A), R1·R2 (B), or D1·R2 (C) duplex and cacodylate buffer. Each heat burst curve is the result of a 5 μL injection of 500 μM drug, with the duplex concentration being 20 μM.

each of the three host duplexes is approximately two drug molecules per duplex. For the D1·R2 hybrid duplex, the ITC-derived binding stoichiometry is consistent with the CD-derived value discussed above.

Further inspection of the data in Table 1 reveals that, for the R1·R2 and D1·R2 duplexes, the affinity (K_a) of paromomycin for the first binding site is substantially greater than the affinity for the second binding site (~44-fold greater for R1·R2 and ~39-fold greater for D1·R2). Recall that our CD studies were consistent with a single mode of paromomycin binding to the D1·R2 duplex (see Figures 3B and C). This observation, coupled with the observed binding stoichiometry of two paromomycin molecules per duplex, suggests that both drug molecules bind to the D1·R2 duplex via a similar mode, even though they exhibit differing affinities for the duplex. The same is likely to be true when R1·R2 serves as the host duplex, since the ITC

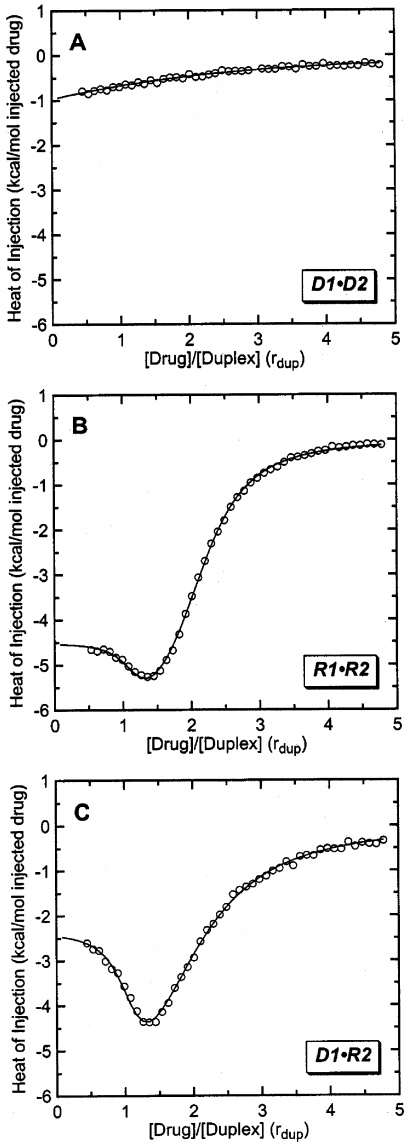

Figure 5. Corrected ITC injection heats plotted as a function of the [drug]/[duplex] ratio (r_{dup}). These heats were derived by integration of the ITC profiles shown in Figure 4, followed by subtraction of the corresponding dilution heats derived from control titrations of drug into buffer alone. The data points reflect the experimental injection heats, while the solid lines reflect the calculated fits of the data. The data in panel A were fit with a model for a single set of binding sites, whereas the data in panels B and C were fit with a model for two independent sets of binding sites.

profiles describing the binding of paromomycin to the D1·R2 and R1·R2 duplexes are similar in nature. Previously reported studies have demonstrated the major groove-directed binding of aminoglycosides to a variety of duplex RNA structures. Thus, it is likely that the mode by which paromomycin binds to the D1·R2 and R1·R2 duplexes is also directed toward the major groove.

A comparison of the K_a values associated with the high-affinity binding of paromomycin to the R1·R2 and D1·R2 duplexes with the corresponding K_a value for paromomycin-D1·D2 complexation reveals the following hierarchy of affinity: R1·R2 > D1·R2 ≫ D1·D2. Specifically, paromomycin binds to the D1·R2 duplex ($K_a = 4.3 \times 10^6$ M^{-1}) with a 187-fold higher affinity than the D1·D2 duplex ($K_a = 2.3 \times 10^4$ M^{-1}) and only a 3.7-fold lower affinity than the R1·R2 duplex

Table 1. ITC-Derived Binding Parameters for the Complexation of Paromomycin with the Three Octamer Duplexes in Cacodylate Buffer at pH 6.0 and a Temperature of 15 °C[a]

duplex	set(s) of sites[b]	N[c]	K_a[d] (M^{-1})	ΔH_{obs}[d] (kcal/mol)
D1·D2	1	1.7	$(2.3 \pm 0.1) \times 10^4$	-2.2 ± 0.1
R1·R2	2	1.1	$(1.6 \pm 0.3) \times 10^7$	-4.5 ± 0.1
		1.1	$(3.6 \pm 0.1) \times 10^5$	-6.9 ± 0.1
D1·R2	2	1.1	$(4.3 \pm 0.4) \times 10^6$	-2.3 ± 0.1
		0.9	$(1.1 \pm 0.1) \times 10^5$	-9.4 ± 0.1

[a] Solution conditions were 10 mM sodium cacodylate, 0.1 mM Na_2EDTA, and sufficient NaCl to bring the total Na^+ concentration to 60 mM. [b] The ITC profiles for paromomycin complexation with the R1·R2 and D1·R2 duplexes were fit with a model for two independent sets of binding sites, whereas the corresponding ITC profile for paromomycin complexation with the D1·D2 duplex was fit with a model for one set of binding sites. [c] N denotes the drug to duplex binding stoichiometry for each set of binding sites that were fit. For each ITC profile, the values of N were fixed during the fitting routine and manually varied to yield the best fit (as reflected by minimization of χ^2). [d] K_a denotes the paromomycin-duplex association constant, while ΔH_{obs} denotes the observed binding enthalpy. The indicated values of K_a and ΔH_{obs} were derived from the fits of the ITC profiles, with the indicated uncertainties reflecting the standard deviations of the experimental data points from the fitted curves.

($K_a = 1.6 \times 10^7$ M^{-1}). Recall that the CD spectra of the R1·R2 and D1·D2 duplexes were characteristic of canonical A- and B-conformations, respectively (Figure 3A). Furthermore, the corresponding CD spectrum of the D1·R2 duplex was consistent with this duplex adopting an A-like conformation (Figure 3B). Hence, our observed hierarchy of paromomycin binding affinity correlates with the extent to which the host duplex adopts an A-like conformation. In other words, both our ITC and CD data are consistent in suggesting that paromomycin is an A-form-specific nucleic acid binding drug.

Binding of Paromomycin to the Three Octamer Duplexes is Linked to the Uptake of a Similar Number of Protons, with the Magnitude of this Number Depending on pH. Our previous studies have indicated that, at pH > 5.5, the binding of paromomycin to an RNA oligonucleotide that models the A-site of E. coli 16 S rRNA is thermodynamically coupled to drug protonation.[38] Recall that the ITC studies described above were conducted at pH 6.0, thereby raising the possibility that the observed paromomycin binding affinities at this pH reflect contributions from binding-linked drug protonation. Thus, it is important to determine whether the binding of paromomycin to the three host duplexes studied here is linked to drug protonation and, if so, to what extent. To this end, we conducted ITC experiments at pH 6.0 and 7.0 using buffers that differ with respect to their heats of ionization (ΔH_{ion}). At pH 6.0, we supplemented our ITC experiments described above, which were conducted in cacodylate buffer, with identical experiments conducted in MES buffer. At pH 7.0, we used cacodylate and PIPES as the two experimental buffers. As indicated in Table 2, both MES and PIPES have different values of ΔH_{ion} than cacodylate. Thus, if the binding of paromomycin to the three duplexes studied here were linked to the uptake of protons, then the observed binding enthalpies (ΔH_{obs}) at a given pH should vary with the buffer employed. Furthermore, the number of protons linked to binding at a specific pH (Δn), as well as the intrinsic binding enthalpy (ΔH_{int}), a value that differs from ΔH_{obs} in that it excludes enthalpic contributions from ionization of

(38) Kaul, M.; Pilch, D. S. *Biochemistry* **2002**, *41*, 7695−7706.

Table 2. Buffer and pH Dependence of the Observed and Intrinsic Enthalpies, as Well as of the Number of Linked Protons, for the Binding of Paromomycin to the Three Octamer Duplexes at 15 °C

duplex	pH	buffer (10 mM)	ΔH_{ion}[a] (kcal/mol)	ΔH_{obs}[b] (kcal/mol)	ΔH_{int}[b] (kcal/mol)	Δn[b] (per drug)
D1·D2	6.0	cacodylate	−0.28	−2.2 ± 0.1	−2.1 ± 0.2	0.18 ± 0.08
D1·D2	6.0	MES	+3.67	−1.5 ± 0.2	−2.1 ± 0.2	0.18 ± 0.08
R1·R2	6.0	cacodylate	−0.28	−4.5 ± 0.1	−4.4 ± 0.1	0.18 ± 0.05
R1·R2	6.0	MES	+3.67	−3.8 ± 0.1	−4.4 ± 0.1	0.18 ± 0.05
D1·R2	6.0	cacodylate	−0.28	−2.3 ± 0.1	−2.2 ± 0.1	0.15 ± 0.05
D1·R2	6.0	MES	+3.67	−1.7 ± 0.1	−2.2 ± 0.1	0.15 ± 0.05
R1·R2	7.0	cacodylate	−0.28	−10.2 ± 0.1	−10.0 ± 0.1	0.63 ± 0.07
R1·R2	7.0	PIPES	+2.69	−8.3 ± 0.1	−10.0 ± 0.1	0.63 ± 0.07
D1·R2	7.0	cacodylate	−0.28	−7.8 ± 0.1	−7.6 ± 0.1	0.71 ± 0.07
D1·R2	7.0	PIPES	+2.69	−5.7 ± 0.1	−7.6 ± 0.1	0.71 ± 0.07

[a] Ionization heats (ΔH_{ion}) at 15 °C for the indicated buffers were calculated using the appropriate values of ΔH_{ion} at 25 °C and the corresponding heat capacity changes of ionization (ΔC_{p-ion}), as determined by H. Fukada and K. Takahashi (1987, unpublished results). The values of ΔH_{ion} at 25 °C that were used in these calculations are as follows: −0.47 kcal/mol for cacodylate, +3.71 kcal/mol for MES, and +2.74 kcal/mol for PIPES. The corresponding values of ΔC_{p-ion} that were used are as follows: −18.64 cal/mol·K for cacodylate, +3.82 cal/mol·K for MES, and +4.54 cal/mol·K for PIPES. [b] The number of binding-linked protons (Δn) and intrinsic binding enthalpies (ΔH_{int}) at 15 °C were calculated using eqs 1a and 1b, as well as the corresponding experimentally observed binding enthalpies (ΔH_{obs}).

the buffer, can be determined by simultaneous solution of the following two equations[39]

$$\Delta H_{obs1} = \Delta H_{int} + \Delta H_{ion1}\Delta n \quad (1a)$$

$$\Delta H_{obs2} = \Delta H_{int} + \Delta H_{ion2}\Delta n \quad (1b)$$

In these equations, the numerical subscripts refer to the different buffers.

Table 2 summarizes the values of Δn and ΔH_{int} associated with the binding of paromomycin to each of the host duplexes at pH 6.0 and 7.0 (as calculated by solution of eq 1a and 1b). Note that, for the R1·R2 and D1·R2 duplexes, the values of ΔH_{obs} listed in Table 2 reflect the observed binding enthalpies associated with the high-affinity binding of paromomycin. Further note the absence of data for paromomycin binding to the D1·D2 duplex at pH 7.0. This omission is due to the weak nature of the paromomycin-D1·D2 interaction at pH 7.0, which precludes us from accurately determining the requisite values of ΔH_{obs} at this pH. Inspection of the data in Table 2 reveals that, at pH values of 6.0 and 7.0, ΔH_{obs} varies with buffer. Specifically, at either pH, ΔH_{obs} is more exothermic in cacodylate buffer than in MES or PIPES. Given the values of ΔH_{ion} for cacodylate, MES, and PIPES at 15 °C (−0.28, +3.67, and +2.69 kcal/mol, respectively),[40] this observation indicates that paromomycin binding to the three host duplexes is coupled to the uptake of protons. This uptake is reflected in the positive values of Δn, which, at pH 6.0, are similar in magnitude for each of the three host duplexes. Specifically, the binding of paromomycin to the D1·D2, R1·R2, and D1·R2 duplexes at pH 6.0 is associated with respective Δn values of +0.18 ± 0.08, +0.18 ± 0.05, and +0.15 ± 0.05, three values that are essentially identical within the limits of the experimental uncertainty. This similarity among Δn values suggests that, at pH 6.0, our observed paromomycin binding affinities reflect similar contributions from binding-linked drug protonation. In other words, the differential affinities exhibited by paromomycin for the three host duplexes are not the result of differential contributions from binding-linked protonation. In a previous communication, we reported that the 3-amino group of paromomycin sulfate has a pK_a value of 7.07, with the remaining four amino groups having pK_a values ≥ 8.25.[41] These pK_a values imply that the 3-amino group is the only amino group on paromomycin that is not fully protonated at pH 6.0. Thus, our observed positive Δn values at pH 6.0 indicate that the binding of paromomycin to each of the three host duplexes is coupled to protonation of the 3-amino group.

Further inspection of the data in Table 2 reveals that, as observed at pH 6.0, the binding of paromomycin to the R1·R2 and D1·R2 duplexes at pH 7.0 is also associated with positive Δn values that are similar in magnitude (+0.63 ± 0.07 and +0.71 ± 0.07, respectively). Note that these Δn values are significantly larger in magnitude than the corresponding values at pH 6.0, an observation indicating a greater of extent of binding-linked drug protonation at pH 7.0 than at pH 6.0. A comparison of the protonation states of the individual amino groups of paromomycin sulfate at pH 7.0 (as predicted by our recently reported NMR-derived pK_a values[41]) with the observed Δn values at this pH suggests that the binding of paromomycin to the R1·R2 and D1·R2 duplexes is coupled to the protonation of not only the 3-amino group, as noted above, but also the 2′- and 2‴-amino groups (pK_a = 8.33 and 8.25, respectively). In the aggregate, our observations are consistent with the binding of paromomycin to both the R1·R2 and D1·R2 duplexes involving interactions between the host duplex and the 3-, 2′-, and 2‴-amino groups of the drug.

Thermodynamic Origins of the Binding Affinity and Specificity Exhibited by Paromomycin. We used the calorimetric data summarized in Tables 1 and 2 to derive complete and buffer-independent thermodynamic profiles for the binding of paromomycin to the three host duplexes studied here at pH 6.0 and 7.0. Specifically, the association constants (K_a) derived from fits of our ITC profiles enabled us to calculate the corresponding binding free energies (ΔG) using the standard relationship

$$\Delta G = -RT\ln K_a \quad (2)$$

These calculated binding free energies, coupled with the intrinsic binding enthalpies (ΔH_{int}) listed in Table 2, allow us to calculate the corresponding entropic contributions to binding ($T\Delta S_{int}$) using the standard relationship

$$T\Delta S = \Delta H - \Delta G \quad (3)$$

The thermodynamic profiles resulting from these calculations are shown in Table 3. Inspection of these data reveals several significant features.

(1) Paromomycin Binding to the D1·R2 Hybrid Duplex Versus the R1·R2 RNA Duplex. At both pH 6.0 and 7.0, the affinity of paromomycin for the R1·R2 RNA duplex is greater than that for the D1·R2 hybrid duplex. Furthermore, this differential binding affinity is enthalpically driven. In fact, the enhanced binding of paromomycin to the R1·R2 duplex occurs

(39) Doyle, M. L.; Louie, G.; Dal Monte, P. R.; Sokoloski, T. D. *Methods Enzymol.* **1995**, *259*, 183−194.
(40) Fukada, H.; Takahashi, K.; Sturtevant, J. M. *Biochemistry* **1987**, *26*, 4063−4068.
(41) Kaul, M.; Barbieri, C. M.; Kerrigan, J. E.; Pilch, D. S. *J. Mol. Biol.* **2003**, *326*, 1373−1387.

Table 3. pH Dependence of the Thermodynamic Profiles for the Binding of Paromomycin to the Three Octamer Duplexes at 15 °C and a Na^+ Concentration of 60 mM

duplex	pH	ΔH_{int}[a] (kcal/mol)	$T\Delta S_{int}$[a] (kcal/mol)	ΔG[b] (kcal/mol)	K_a[c] (M^{-1})
D1·D2	6.0	-2.1 ± 0.2	$+3.7 \pm 0.3$	-5.8 ± 0.1	$(2.3 \pm 0.1) \times 10^4$
R1·R2	6.0	-4.5 ± 0.1	$+5.0 \pm 0.2$	-9.5 ± 0.1	$(1.6 \pm 0.3) \times 10^7$
D1·R2	6.0	-2.2 ± 0.1	$+6.5 \pm 0.2$	-8.7 ± 0.1	$(4.3 \pm 0.4) \times 10^6$
D1·D2[d]	7.0	ND	ND	ND	ND
R1·R2	7.0	-10.0 ± 0.1	-1.7 ± 0.2	-8.3 ± 0.1	$(2.1 \pm 0.1) \times 10^6$
D1·R2	7.0	-7.6 ± 0.1	0.4 ± 0.2	-8.0 ± 0.1	$(1.2 \pm 0.1) \times 10^6$

[a] ΔH_{int} and ΔS_{int} are the intrinsic binding enthalpy and entropy, respectively. These intrinsic binding parameters are independent of the buffer employed. Values of ΔH_{int} were determined as described in the text, whereas values of $T\Delta S_{int}$ were determined using eq 3. [b] ΔG is the binding free energy, as determined using eq 2. [c] Association constants were derived from fits of ITC profiles acquired in cacodylate buffer. Note that these association constants are similar in magnitude to those derived from fits of the corresponding ITC profiles acquired in either MES or PIPES buffer. [d] ND denotes not determinable, due to the weak nature of the paromomycin-D1·D2 interaction at pH 7.0.

despite a less favorable (positive) binding entropy, which is overcompensated by a more favorable (negative) enthalpic contribution to binding. In other words, paromomycin enthalpically discriminates between the RNA duplex and the DNA·RNA hybrid duplex. Recall that our CD data (see Figure 3) were consistent with paromomycin binding to the D1·R2 hybrid duplex being accompanied by a conformational transition from an A-like to a more canonical A-conformation. Such a conformational change is associated with an enthalpy-driven energetic penalty[42−44] and may therefore account, at least in part, for the enthalpic origins of the reduced affinity exhibited by paromomycin for the D1·R2 hybrid duplex relative to the R1·R2 RNA duplex. Note that, at pH 6.0, paromomycin binds to the R1·R2 duplex with a 0.8 kcal/mol greater affinity than to the D1·R2 duplex, but only a 0.3 kcal/mol greater affinity at pH 7.0. Thus, the extent to which paromomycin discriminates between the R1·R2 and D1·R2 duplexes appears to decrease with increasing pH.

(2) Paromomycin Binding to the R1·R2 RNA and D1·R2 Hybrid Duplexes versus the D1·D2 DNA Duplex. At pH 6.0, paromomycin binds to the D1·D2 DNA duplex with a 3.7 kcal/mol lower affinity than the R1·R2 RNA duplex and a 2.9 kcal/mol lower affinity than the D1·R2 hybrid duplex. The 3.7 kcal/mol enhanced affinity of paromomycin for the R1·R2 duplex relative to the D1·D2 duplex is 65% enthalpic and 35% entropic in origin, whereas the 2.9 kcal/mol enhanced affinity of paromomycin for the D1·R2 duplex relative to the D1·D2 duplex is entropically driven. By the same reasoning discussed in the previous section, the lack of an enthalpic contribution to the preferential binding of paromomycin to D1·R2 hybrid duplex versus the D1·D2 DNA duplex may reflect the conformational change in the D1·R2 duplex that is induced by the binding of the drug. Numerous structural studies of aminoglycoside-RNA complexes have revealed that these drugs bind in the major grooves of the host RNA structures.[10−17,19,45−48] Thus, it is likely that the binding of paromomycin to the R1·R2 and D1·R2 duplexes, which our CD data indicate preexist in or adopt A-conformations, reflects a major groove-directed mode of interaction. However, the same is not likely to be true for the paromomycin-D1·D2 interaction. Our CD data revealed the D1·D2 duplex to adopt the B-form (Figure 3A), with paromomycin binding inducing little or no change in this conformation (not shown). The wide and shallow nature of the major groove in B-form DNA[23] makes it a poor substrate for drug binding. Thus, the comparatively weak binding of paromomycin to the D1·D2 duplex relative to the R1·R2 and D1·R2 duplexes is probably not directed to the major groove of the DNA. Instead, it may reflect an electrostatically driven nonspecific mode of interaction with the DNA. In support of this possibility, raising the Na^+ concentration above 60 mM essentially abolishes the binding of paromomycin to the D1·D2 duplex (not shown).

(3) Thermodynamics of Paromomycin Binding to the R1·R2 and D1·R2 Duplexes is Modulated by pH. Paromomycin binds to the R1·R2 duplex with a 1.2 kcal/mol higher affinity at pH 6.0 than at pH 7.0. Similarly, paromomycin binds to the D1·R2 duplex with a 0.7 kcal/mol higher affinity at pH 6.0 than at pH 7.0. Thus, increasing pH reduces the affinity of paromomycin for the two host duplexes. Note that, in both cases, the pH-induced reduction in paromomycin binding affinity occurs despite a substantially more favorable (exothermic) binding enthalpy. In other words, the reduced affinity is entropic in origin. These results are consistent with our observation described above that the binding of paromomycin to the R1·R2 and D1·R2 duplexes at pH 6.0 and 7.0 is linked to protonation of drug amino groups. The protonation of amino groups is known to be an exothermic process. For example, protonation of the 2-amino group of D-glucosamine is associated with an enthalpy change of -5.3 kcal/mol.[49] While being enthalpically favorable, protonation reactions are entropically costly, and it is this cost that most likely accounts for the entropic origins of the reduced affinity exhibited by paromomycin for the R1·R2 and D1·R2 duplexes at pH 7.0 relative to pH 6.0.

In the preceding sections, we used an array of spectroscopic and calorimetric techniques to demonstrate that paromomycin can bind to a DNA·RNA hybrid duplex, while causing the host duplex to undergo a transition from an A-like to a more canonical A-conformation. This observation raises the question as to the potential biological impact of aminoglycoside complexation with DNA·RNA hybrid structures. In the section that follows, we describe experiments probing the impact of paromomycin binding to the D1·R2 hybrid duplex on the activities of two RNA processing enzymes, RNase A from bovine pancreas and recombinant RNase H from *E. coli*.

Paromomycin Binding Inhibits both RNase A- and RNase H-Mediated Cleavage of the RNA Strand in the D1·R2 Hybrid Duplex. We determined the impact of paromomycin binding to the D1·R2 hybrid duplex on the RNA cleavage catalyzed by RNase A and RNase H. At Na^+ concentrations <100 mM, RNase A cleaves RNA in either its single-stranded state or when hybridized to a complementary strand of RNA

(42) Ivanov, V. I.; Minchenkova, L. E. *Molek. Biol. (USSR)* **1994**, *28*, 1258−1271.
(43) Ivanov, V. I.; Minchenkova, L. E. *Mol. Biol. (USSR)* **1995**, *28*, 780−788.
(44) Jayaram, B.; Sprous, D.; Young, M. A.; Beveridge, D. A. *J. Am. Chem. Soc.* **1998**, *120*, 10 629−10 633.
(45) Patel, D. J.; Suri, A. K.; Jiang, F.; Jiang, L.; Fan, P.; Kumar, R. A.; Nonin, S. *J. Mol. Biol.* **1997**, *272*, 645−664.
(46) Hermann, T.; Westhof, E. *J. Mol. Biol.* **1998**, *276*, 903−912.
(47) Recht, M. I.; Douthwaite, S.; Puglisi, J. D. *EMBO J.* **1999**, *18*, 3133−3138.
(48) Lynch, S. R.; Puglisi, J. D. *J. Mol. Biol.* **2001**, *306*, 1037−1058.
(49) Miyamoto, S.; Kazuko, M. *Kyoritsu Yakka Daigaku Kenkyû Nempô* **1958**, *4*, 12−16.

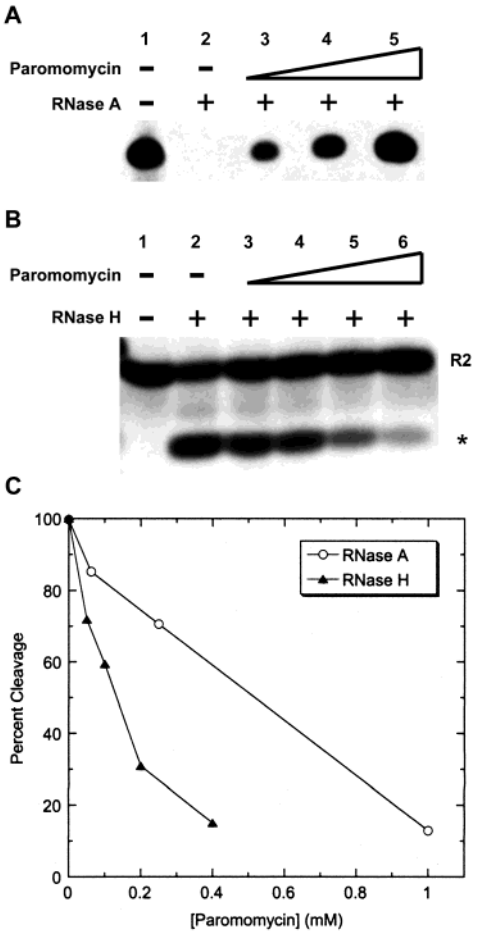

Figure 6. (A) Denaturing 15% polyacrylamide gel showing bovine pancreas RNase A cleavage of the D1·R2 duplex (0.5 μM) in the absence or presence of paromomycin. All the lanes contain enzyme except lane 1. The paromomycin concentrations in lanes 2, 3, 4, and 5 are 0, 62.5, 250, and 1000 μM, respectively. (B) Denaturing 15% polyacrylamide gel showing *E. coli* RNase H cleavage of the D1·R2 duplex (0.5 μM) in the absence or presence of paromomycin. All the lanes contain enzyme except lane 1. The paromomycin concentrations in lanes 2, 3, 4, 5, and 6 are 0, 50, 100, 200, and 400 μM, respectively. The band corresponding to the intact R2 strand is so indicated, whereas an asterisk denotes the RNase H cleavage product. (C) Quantitation of the extent of both RNase A- and RNase H-mediated cleavage as a function of paromomycin concentration.

or DNA.[50] By contrast, RNase H only cleaves RNA that is hybridized to DNA.[50] The RNase A and RNase H cleavage profiles that we obtained are shown in Figure 6A and B, respectively. Note that paromomycin inhibits both RNase A- and RNase H-mediated cleavage of the RNA strand in the hybrid duplex, with the extent of this inhibition being dependent on the concentration of the drug. Specifically, under the solution conditions employed (5 mM Mg^{2+}, pH 6.0), RNase A cleavage is inhibited by ~87% at a [paromomycin]/[duplex] ratio of 2000, with RNase H cleavage being inhibited by ~85% at a [paromomycin]/[duplex] ratio of 800 (Figure 6C). Thus, the binding of paromomycin to the host hybrid duplex is capable of inhibiting the activities of both RNA processing enzymes, with the efficacy of inhibition being greater for RNase H than for RNase A. Significantly, the activities of RNase A and RNase H are required for the ultimate expression of the functions associated with the nucleic acids that serve as their substrates. Hence, our observations open the door to the possibility of achieving desired biological endpoints by targeting specific DNA·RNA hybrid or other A-like nucleic acid structures with small molecules.

(50) Struhl, K. In *Current Protocols in Molecular Biology*; Ausubel, F. M., Brent, R., Kingston, R. E., Moore, D. D., Seidman, J. G., Smith, J. A., Struhl, K., Eds.; John Wiley & Sons: New York, 1993; Vol. 1, pp 3.13.11−13.13.13.

Concluding Remarks

We have used a combination of spectroscopic and calorimetric techniques to characterize and contrast the binding of the aminoglycoside paromomycin to a DNA·RNA hybrid duplex relative to RNA·RNA and DNA·DNA duplexes of the same sequence. Our studies reveal that paromomycin binds to A-form nucleic acids with a significantly higher affinity than B-form nucleic acids. In this connection, we show that paromomycin binding to the DNA·RNA hybrid duplex induces a transition from an A-like to a more canonical A-conformation. We also show that the binding of paromomycin to the DNA·RNA duplex inhibits both RNase A- and RNase H-mediated cleavage of the RNA strand in the target duplex. As noted above, this observation highlights the potential of using rationally designed molecules to target specific DNA·RNA structures, thereby modulating specific biological processes in a desired manner. In this connection, Chaires and co-workers have identified a number of intercalating ligands that uniquely recognize the poly(rA)·poly(dT) hybrid duplex.[25] Note that the structures and stabilities of DNA·RNA hybrid duplexes can vary considerably with the sequence composition of the DNA and RNA strands.[33] These sequence-dependent variations in structure and stability offer the possibility for increased specificity in the targeting of DNA·RNA hybrid structures.

Reverse transcriptase-mediated RNase H processing of DNA·RNA hybrid domains is essential for the replication of retroviruses.[26] Thus, one potential therapeutic application of drugs that target specific DNA·RNA structures is the inhibition of retroviral replication by interfering with the RNase H activity of reverse transcriptase.[24,25] Recall that the sequence of the RNA strand in the DNA·RNA hybrid duplex studied here (D1·R2) is derived from the HIV-1 genome, consisting of the four bases at the 3′-end of the U5 region and the four bases at the 5′-end of the primer binding site (PBS).[27] The ability of paromomycin to inhibit the processing of the D1·R2 duplex by *E. coli* RNase H raises the possibility of using aminoglycosides or other DNA·RNA-targeting agents to inhibit the RNase H activities of retroviral reverse transcriptases, thereby inhibiting viral replication. Significantly, such an antiretroviral approach should not be compromised by the genomic instabilities exhibited by many retroviruses.

Acknowledgment. This work was supported by grants from the National Institutes of Health (GM 31483, GM48802, and GM60484) and the American Cancer Society (RPG# 99-153-04-CDD). The calorimetric instrumentation was purchased through funds from NIH grant S10 RR15959-01. D. S. Pilch was supported, in part, by a Young Investigator Award from the Cancer Institute of New Jersey.

JA021371D